Postsynaptic GABAB-receptor mediated currents in diverse dentate gyrus interneuron types

Received: 8 March 2024 | Revised: 24 June 2024 | Accepted: 19 July 2024

DOI: 10.1002/hipo.23628

RESEARCH ARTICLE

WILEY

Postsynaptic $GABA_B$-receptor mediated currents in diverse dentate gyrus interneuron types

Claudius E. Degro[1] | Imre Vida[1] | Sam A. Booker[1,2,3]

[1]Institute for Integrative Neuroanatomy, Charité—Universitätmedizin Berlin, Berlin, Germany

[2]Centre for Discovery Brain Sciences, University of Edinburgh, Edinburgh, UK

[3]Simons Initiative for the Developing Brain, University of Edinburgh, Edinburgh, UK

Correspondence
Imre Vida, Institute for Integrative Neuroanatomy, Charité—Universitätmedizin Berlin, Berlin, Germany.
Email: imre.vida@charite.de

Sam A. Booker, Simons Initiative for the Developing Brain, Centre for Discovery Brain Sciences, University of Edinburgh, Edinburgh, UK.
Email: sbooker@ed.ac.uk

Funding information
Simons Foundation Autism Research Initiative; Deutsche Forschungsgemeinschaft

Abstract

The processing of rich synaptic information in the dentate gyrus (DG) relies on a diverse population of inhibitory GABAergic interneurons to regulate cellular and circuit activity, in a layer-specific manner. Metabotropic $GABA_B$-receptors ($GABA_B$Rs) provide powerful inhibition to the DG circuit, on timescales consistent with behavior and learning, but their role in controlling the activity of interneurons is poorly understood with respect to identified cell types. We hypothesize that $GABA_B$Rs display cell type-specific heterogeneity in signaling strength, which will have direct ramifications for signal processing in DG networks. To test this, we perform *in vitro* whole-cell patch-clamp recordings from identified DG principal cells and interneurons, followed by $GABA_B$R pharmacology, photolysis of caged GABA, and extracellular stimulation of endogenous GABA release to classify the cell type-specific inhibitory potential. Based on our previous classification of DG interneurons, we show that postsynaptic $GABA_B$R-mediated currents are present on all interneuron types albeit at different amplitudes, dependent largely on soma location and synaptic targets. $GABA_B$Rs were coupled to inwardly-rectifying $K+$ channels that strongly reduced the excitability of those interneurons where large currents were observed. These data provide a systematic characterization of $GABA_B$R signaling in the rat DG to provide greater insight into circuit dynamics.

KEYWORDS
dentate gyrus, $GABA_B$ receptors, inhibition, interneuron

1 | INTRODUCTION

The mammalian dentate gyrus (DG) is the main input region of the hippocampus and receives rich spatial information from the entorhinal cortex via the perforant path (Borzello et al., 2023; Fernández-Ruiz et al., 2021). A main function of the DG is assumed to be orthogonalization and sparsification of the rich cortical code which is then played forward onto downstream CA3 pyramidal cells (Schmidt-Hieber & Nolan, 2017). These processes rely on a combination of excitation and inhibition (Morales et al., 2021; Srivastava et al., 2008), the latter of which is provided by a heterogeneous population of local interneurons (INs) (Booker & Vida, 2018; Freund & Buzsáki, 1996; Houser, 2007; Hosp et al., 2014). We have recently shown that the diversity of DG INs is greater than previously believed, with over 13 cell types that occupy unique niches within the local circuit to control the excitability of dentate granule cells (DGCs) (Degro et al., 2022). The activity of these INs is required for appropriate processing of spatial information, thus determining their inhibition mechanisms is fundamental to understanding the function of DG circuits.

Imre Vida and Sam A. Booker co-corresponding authors.

Local neuronal inhibition is mainly mediated by the synaptic release of GABA, which activates fast ionotropic $GABA_A$ receptors ($GABA_ARs$) and slow metabotropic $GABA_B$ receptors ($GABA_BRs$) (Bettler et al., 2004; Dutar & Nicoll, 1988). $GABA_ARs$ have been shown to play a central role in controlling information flow through the DG on short timescales (Bartos et al., 2001; Bartos et al., 2007; Vida et al., 2006), contributing to generation of local oscillations and sparsification of DGC output. However, while small in amplitude, the slow kinetics of $GABA_BR$ signaling provide powerful, hyperpolarizing inhibition to the somatodendritic compartments of neurons (Bettler et al., 2004), and thus may control activity over longer timescales. Indeed, $GABA_BRs$ have been linked to spatial memory (Brucato et al., 1996), synaptic plasticity (Davies et al., 1991; Mott & Lewis, 1991), and can facilitate DGC output by directly inhibiting DG INs (Foster et al., 2013). Earlier immunocytochemical studies have shown that DG INs do possess $GABA_BRs$ (Kulik et al., 2002; Kulik et al., 2003), but this has only been functionally assessed in few, minimally characterized cell types (Mott et al., 1999) and which likely only account for a fraction of DG IN types (Degro et al., 2022). In a series of studies, we have shown that $GABA_BRs$ control the activity of INs in CA1 of the hippocampus, with respect to cell type, current density, and receptor kinetics (Booker et al., 2013, 2017, 2018, 2020). Whether $GABA_BRs$ provide inhibition to all the diverse types of DG INs remains unexplored.

In this study, we performed a systematic analysis of postsynaptic $GABA_BR$-mediated currents in diverse DG IN types, as classified in our recent study (Degro et al., 2022), to determine whether IN-type differences in $GABA_BR$-mediated signaling exist in the DG. For this, we combined *in vitro* whole-cell patch-clamp recordings with extracellular stimulation, photolysis, and direct pharmacological receptor activation. We show that $GABA_BR$ signaling displays cell type-dependent diversity in the DG, which may account for IN-specific circuit dynamics and thus control information processing over a range of physiological timescales.

2 | METHODS

2.1 | Acute slice preparation

Acute brain slices were obtained from 18 to 26 day-old male and female Wistar rats, expressing a yellow fluorescence protein (YFP, "Venus variant") under the vesicular GABA transporter promoter (Uematsu et al., 2008). After deep sedation with isoflurane, rats were decapitated and the brains rapidly removed into ice-cold carbogenated (95% O_2/5% CO_2) sucrose-modified artificial cerebrospinal fluid (sucrose-ACSF; in mM: 87 NaCl, 2.5 KCl, 25 $NaHCO_3$, 1.25 NaH_2PO_4, 25 Glucose, 75 Sucrose, 1 Na_2-Pyruvate, 1 Na_2-Ascorbate, 7 $MgCl_2$, 0.5 $CaCl_2$). Transverse hippocampal slices (300 µm nominal thickness) were then prepared in ice-cold sucrose-ACSF using an oscillating blade vibratome (VT1200s, Leica, Germany) as previously described (Booker et al., 2014). Slices were collected at 5 to 8 mm from the dorsal surface of the brain. Subsequently, brain slices were kept in submerged storage chambers containing warmed sucrose-ACSF (35 °C) for 30 minutes before storage at room temperature (20 °C) until recording. All animal procedures were performed in accordance with local (LaGeSo, Berlin, T 0215/11) and national guidelines (German Animal Welfare Act).

2.2 | Whole-cell patch-clamp recordings

Electrophysiological recordings were performed as previously described (Degro et al., 2022). In this study focusing on $GABA_BR$ effects, 59 recorded neurons were included from our previous study, in which we had analyzed neuronal morphology and baseline intrinsic electrophysiological properties to establish a new classification of DG INs (Degro et al., 2022). An additional 26 neurons were recorded specifically for this study. For both data sets $GABA_BR$ signaling and its effect on neuronal excitability were examined.

In brief, hippocampal slices were transferred to a submerged recording chamber and superfused with carbogenated, normal ACSF (in mM: 125 NaCl, 2.5 KCl, 25 $NaHCO_3$, 1.25 NaH_2PO_4, 25 Glucose, 1 Na_2-Pyruvate, 1 Na_2-Ascorbate, 1 $MgCl_2$, 2 $CaCl_2$) at a near physiological temperature (32 ± 0.4 °C) using an inline heater (SuperTech, Switzerland). The flow rate was set to 10–12 mL/min to allow improved oxygenation (Hájos & Mody, 2009). Slices were visualized with an upright microscope (BX-50, Olympus, Hamburg, Germany) equipped with a 40× water immersion objective lens (N.A. 0.8) and YFP-positive neurons were selected for electrophysiological recordings in a quasi-random manner across all layers of the DG. YFP-negative neurons within the GCL, that is, DGCs, were collected as a reference population. Whole-cell patch-clamp recordings were performed using a MultiClamp 700B amplifier (Molecular Devices, USA). Recording pipettes were pulled from borosilicate glass capillaries (2 mm outer/1 mm inner diameter, Hilgenberg, Germany) on a horizontal electrode puller (P-97, Sutter Instruments, CA, USA) with pipette resistances of 3–5 MΩ when filled with intracellular solution (in mM: 130 K-gluconate, 10 KCl, 2 $MgCl_2$, 10 EGTA, 10 HEPES, 2 Na_2-ATP, 0.3 Na_2-GTP, 1 Na_2-phosphocreatine and 0.1% Biocytin; 290–310 mOsm). Signals were filtered online at 10 kHz using the built-in 4-pole Bessel filter of the MultiClamp amplifier and digitized and recorded at 20 kHz (NI USB-6212 BNC, National Instruments, Berkshire, UK) using WinWCP software (courtesy of John Dempster, Strathclyde University, Glasgow, UK). Data analysis was performed offline using the open-source Stimfit software package (Guzman et al., 2014; http://www.stimfit.org).

2.3 | Characterization of $GABA_BR$-mediated currents

$GABA_BR$-mediated currents were characterized in voltage-clamp mode at −60 mV in the presence of DNQX (10 µM), DL-AP5 (50 µM) and Gabazine (10 µM) in the perfusing ACSF. Pharmacologically isolated $GABA_BR$-mediated inhibitory postsynaptic currents (IPSCs) were then elicited via endogenous (extracellular stimulation) or exogenous

(photolysis of caged-GABA) GABA release. Extracellular stimulation was delivered to the apical neuropil via a glass monopolar electrode (patch pipettes filled with 2 M NaCl, pipette resistance = 0.1 MΩ) and $GABA_BR$-mediated IPSCs evoked in response to 200 Hz trains of up to 5 stimuli (200 μs duration, 50 V amplitude). Kinetic properties of $GABA_BR$ IPSCs were determined from average traces (minimum 8 individual traces) where the IPSC amplitude was greater than 5 pA.

Local GABA release was achieved by photolysis of the photolabile caged-GABA compound Rubi-GABA (20 μM) applied to the bath (5 min wash-in; Degro et al., 2015). Photorelease of GABA was induced by brief flashes (200 ms flash duration, 2 min inter-flash interval) of 470 nm monochromatic light centered over the soma and capturing the entire visual field (OptiLED, Cairn Scientific, Kent, UK). In some recordings, this photolysis produced a fast transient current, therefore responses recorded in the presence of CGP-55,845 (CGP, 5 μM) were subtracted from the control response for further analyses (average value of three individual traces). Decay-time constants of the $GABA_BR$-mediated response were calculated by fitting a mono-exponential function (offset fixed to baseline) to the decay of the induced current. To assess the whole-cell contingent of $GABA_BR$-mediated currents, the canonical agonist baclofen (10 μM) was applied to the bath for 5 min in all conducted experiments. To test that the baclofen-induced current was specific to $GABA_BRs$, the selective $GABA_BR$ antagonist CGP was subsequently bath-applied. The pharmacologically induced currents produced by baclofen and CGP were measured as the difference between peak holding current (over 2 min) and control level (measured over 2 min prior to drug wash-in). Finally, desensitization of baclofen-induced $GABA_BR$-mediated currents was assessed as the ratio between the peak response and the holding current at the end of the 5 min wash-in (measured over 0.5 min).

2.4 | Characterization of passive and active membrane properties

Physiological properties of neurons were assessed in whole-cell configuration in the presence of DNQX, DL-AP5, and Gabazine, and calculated under control conditions before and during baclofen-induced $GABA_BR$ activation and during antagonism with CGP. Resting membrane potential (V_m) was first measured immediately after breakthrough and subsequently after baclofen and CGP wash-in at zero-current level in current-clamp mode. Input resistance (R_{in}) was calculated in voltage-clamp mode at −60 mV based on the average response of −5 mV pulses (20 ms duration, 10-trace average) assessing the change in current between baseline and steady-state current at the end of the pulse. Membrane capacitance (C_m) was determined in the same experimental protocol by fitting a bi-exponential function (offset fixed to baseline) to the decay of the current induced by the −5 mV pulse following the equation:

$$C_m = \tau_w{}^* (1/R_s + 1/R_{in})$$

with τ_w defined as the weighted time constant and R_s as the series resistance.

Action potentials (APs) were analyzed under all three conditions (control, baclofen, CGP) in current-clamp mode based on hyper-to depolarizing current steps ranging from −250 to 250 pA followed by a last 500 pA pulse (50 pA steps, 500 ms duration). AP discharge frequency was defined as the number of events overshooting 0 mV over the 500 ms trace of depolarizing pulses. For AP analyses, the average of three individual traces was used for further analysis, and liquid junction potential was not corrected.

2.5 | Visualization, imaging and reconstruction

Visualization of the recorded neurons was performed as previously described (Degro et al., 2022). Briefly, after obtaining an outside-out patch at the end of each recording, slices were fixed immediately with 4% paraformaldehyde (PFA) in 0.1 M phosphate buffer (PB), overnight at 4°C. Specimens were then rinsed repeatedly in PB prior to incubation with Alexa Fluor 647-conjugated streptavidin (1:1000, Invitrogen, Dunfermline, UK), diluted in PB containing 0.1% Triton-X100 and 0.05% NaN_3, overnight at 4°C. Finally, slices were mounted on glass slides surrounded by a 300 μm thick agar spacer in a polymerizing mounting medium (Fluoromount-G, Southern Biotech, AL, USA) before cover-slipping. Recorded neurons were visualized on a laser scanning confocal microscope (FluoView 1000, Olympus) with either 20× (N.A 0.75) or oil-immersion 60× (N.A 1.3) objective lenses for reconstruction and type classification. Complete 3D images of the full cell structure were obtained by combining multiple image stacks, collected along the *Z*-axis of the cells (0.5 or 1 μm steps, 4 μs pixel dwell time, 4-megapixel resolution) using the FIJI software package (http://fiji.org). Neurons were then reconstructed with the semi-automatic Simple Neurite Tracer plug-in for FIJI (Longair et al., 2011). Included neurons that have not been rigorously identified based on our prior morpho-physiological cluster analysis (Degro et al., 2022), have been allocated to the existing IN clusters using their morphometric structures.

2.6 | Chemicals and pharmacological tools

Chemicals were purchased from either Sigma Aldrich (Munich, Germany) or Carl Roth (Karlsruhe, Germany) and biocytin was obtained from Life Technologies (Dunfermline, UK). Drugs were purchased from Abcam Biochemicals (Cambridge, UK) or Tocris Bioscience (Bristol, UK). Working concentrations were prepared fresh in normal ACSF on each experimental day from 1000-fold stock concentrations stored at −80°C: DNQX 10 μM, DL-AP5 50 μM, Gabazine (SR-95531) 10 μM, Rubi-GABA 20 μM, CGP-55,845 5 μM and baclofen 10 μM.

2.7 | Statistical analysis

Statistical analysis was performed with GraphPad Prism 9.3.0 (GraphPad Software, CA USA). Group data were compared with either

the Kruskal–Wallis test (KW) combined with Dunn's post-test or repeated measures one-way ANOVA with Bonferroni's multiple comparison post-test to establish group differences. Paired data was analyzed with the Wilcoxon signed-rank test or with Friedman's test combined with Dunn's post-test. Data are shown as mean ± SD throughout, unless stated otherwise, with the data of individual replicates shown overlaid. For most cell types only 1–2 cells per animal were recorded, thus it was not possible to estimate intra-animal variability, therefore all statistics were performed on cell-averaged data. All rats used for this study were selected at random from the home-cage and data were not separated by sex. All data were analyzed prior to assignation to cell type groups, to prevent potential bias.

3 | RESULTS

3.1 | Pharmacologically evoked $GABA_BR$-mediated currents are not uniform among DG IN types

Our primary aim was to determine the contribution of postsynaptic $GABA_BR$-mediated currents based on our previous classification of DG INs based on morpho-electric properties (Figure 1a; Degro et al., 2022). In the 13 IN types previously identified, we noted three major classes of DG INs: perisomatic-targeting (PT) INs with somata in and around the granule cell layer, and dendrite-targeting INs with somata in the hilus (HI), or molecular layer (ML).

To assess the magnitude of postsynaptic $GABA_BR$-mediated currents in these various DG IN types, we first characterized the effect of pharmacological activation by bath application of the canonical $GABA_BR$ agonist baclofen (10 μM). Whole-cell recordings were performed from YFP-expressing INs in acute slices, compared to DGCs. Recordings were obtained in the presence of DNQX (10 μM), DL-AP5 (50 μM), and Gabazine (10 μM), and the whole-cell current was monitored. We first assessed these baclofen-induced currents in DGCs ($n = 8$ cells), as these neurons are known to express high levels of functional postsynaptic $GABA_BRs$ (Degro et al., 2015; Lüscher et al., 1997; Mott et al., 1999). Consistent with these studies, wash-in of baclofen produced prominent outward currents in all DGCs tested. Subsequent application of the potent and selective $GABA_BR$ antagonist CGP-55,845 (CGP, 5 μM) blocked this baclofen current and often produced a small undershoot (Figure 1b)—indicative of tonic $GABA_BR$ activation (Canning & Leung, 2000). Similar currents were observed in PT basket and axo-axonic cells (BC/AAC, $n = 9$ cells), as well as in dendritic inhibitory hilar commissural-associational pathway associated (HICAP, $n = 7$ cells) and ML perforant pathway associated (MOPP, $n = 7$ cells, Figure 1b) cells. Interestingly, baclofen-induced currents smaller than those of DGCs were observed in hilar perforant pathway-associated (like) INs (HIPP/L, $n = 6$ cells, Figure 1b). In all tested INs, baclofen-induced currents (where present) were blocked by bath application of the selective $GABA_BR$ antagonist CGP and often revealed a small undershoot. Time-course plots of baclofen-induced currents for other DG IN types are shown in the Supporting Information Figure 1.

To quantitatively compare the baclofen-induced whole-cell currents in the diverse DG IN types, we next measured the peak outward current produced in recorded neurons, which typically occurred 2–3 min after bath application (Figure 2a).

While most IN types showed baclofen-induced whole-cell currents (Figure 2b), there was substantial variability between groups when compared to DGCs ($H = 33.1$, $p = 0.0003$, KW). Consistent with our previous findings in hippocampal subfield CA1 (Booker et al., 2013), BC/AACs ($n = 11$ cells) possessed baclofen-induced currents of 60.8 ± 28.2 pA comparable to that of DGCs (48.9 ± 20.5 pA, $Z = 0.91$, $p > .99$, $n = 17$ cells, KW, Dunn's). Most other IN types displayed similar baclofen-induced current amplitudes, with the exception of HIPP/L cells (20.4 ± 16.4 pA, $Z = 2.96$, $p = .03$, $n = 7$ cells, KW, Dunn's, compared to DGCs) and hilar medial perforant pathway associated (HIMPP) cells (16.7 ± 8.8 pA, $Z = 3.33$, $p = .009$, $n = 6$ cells, KW, Dunn's, compared to DGCs) which had significantly smaller baclofen-induced peak currents than DGCs.

Absolute current amplitudes can be confounded by differences in neuronal surface area (Spruston & Johnston, 1992). Therefore, we next normalized the baclofen-induced current amplitudes to cell capacitance for each neuron (Figure 2c), as capacitance shows a linear relationship with dendritic length for all DG INs (Supporting Information Figure 2). This analysis confirmed the heterogeneity in baclofen current-density of DG cell types ($H = 55.9$, $p < .0001$, KW). As for the absolute current, BC/AACs showed an average current-density that was equivalent to DGCs (BC/AAC: 0.61 ± 0.43 pA/pF vs. DGCs: 0.60 ± 0.45 pA/pF, $Z = 0.33$, $p > .99$, KW, Dunn's). HIPP/L cells (0.17 ± 0.12 pA/pF, $Z = 2.99$, $p = 0.03$, $n = 7$ cells, KW, Dunn's, compared to DGCs) and HIMPP cells (0.15 ± 0.04 pA/pF, $Z = 3.18$, $p = .01$, $n = 6$ cells, KW, Dunn's, compared to DGCs) displayed significantly lower average current-densities than DGCs. HICAP, total molecular layer (TML), and ML commissural-associational pathway associated (MOCAP) cells also tended to have lower average current-densities, albeit not significantly so (HICAP: 0.33 ± 0.17 pA/pF, $Z = 1.86$, $p = .63$, $n = 11$ cells; TML: 0.34 ± 0.18 pA/pF, $Z = 1.72$, $p = .86$, $n = 12$ cells; MOCAP: 0.38 ± 0.19 pA/pF, $Z = 0.71$, $p > .99$, $n = 3$ cells, KW, Dunn's, all compared to DGCs). In contrast, subiculum projecting I/II (SPI/II) cells possessed a significantly higher average current-density than DGCs (1.1 ± 0.55 pA/pF, $Z = 2.81$, $p = .049$, $n = 12$ cells, KW, Dunn's). The remaining ML IN types, MOPP cells and neurogliaform cells (NGFCs) also revealed average current-densities that were larger than measured in DGCs, however not significantly (MOPP: 0.81 ± 0.25 pA/pF, $Z = 1.80$, $p = .72$, $n = 8$ cells; NGFC: 0.96 ± 0.46 pA/pF, $Z = 1.20$, $p > .99$, $n = 3$ cells, KW, Dunn's, all compared to DGCs).

Postsynaptic $GABA_BR$-mediated currents can undergo rapid desensitization due to internalization of the receptor, in a process believed to be regulated by potassium channel tetramerization domain 12 (KCTD12; Booker et al., 2017; Fritzius et al., 2017). To assess $GABA_BR$ desensitization, we measured baclofen-induced currents 5 minutes after the start of bath application (Figure 2a), which were then compared to the peak response. We observed modest desensitization in DGCs (17.6% ± 14.3% reduction, $W = 36.0$, $p = .008$, $n = 8$

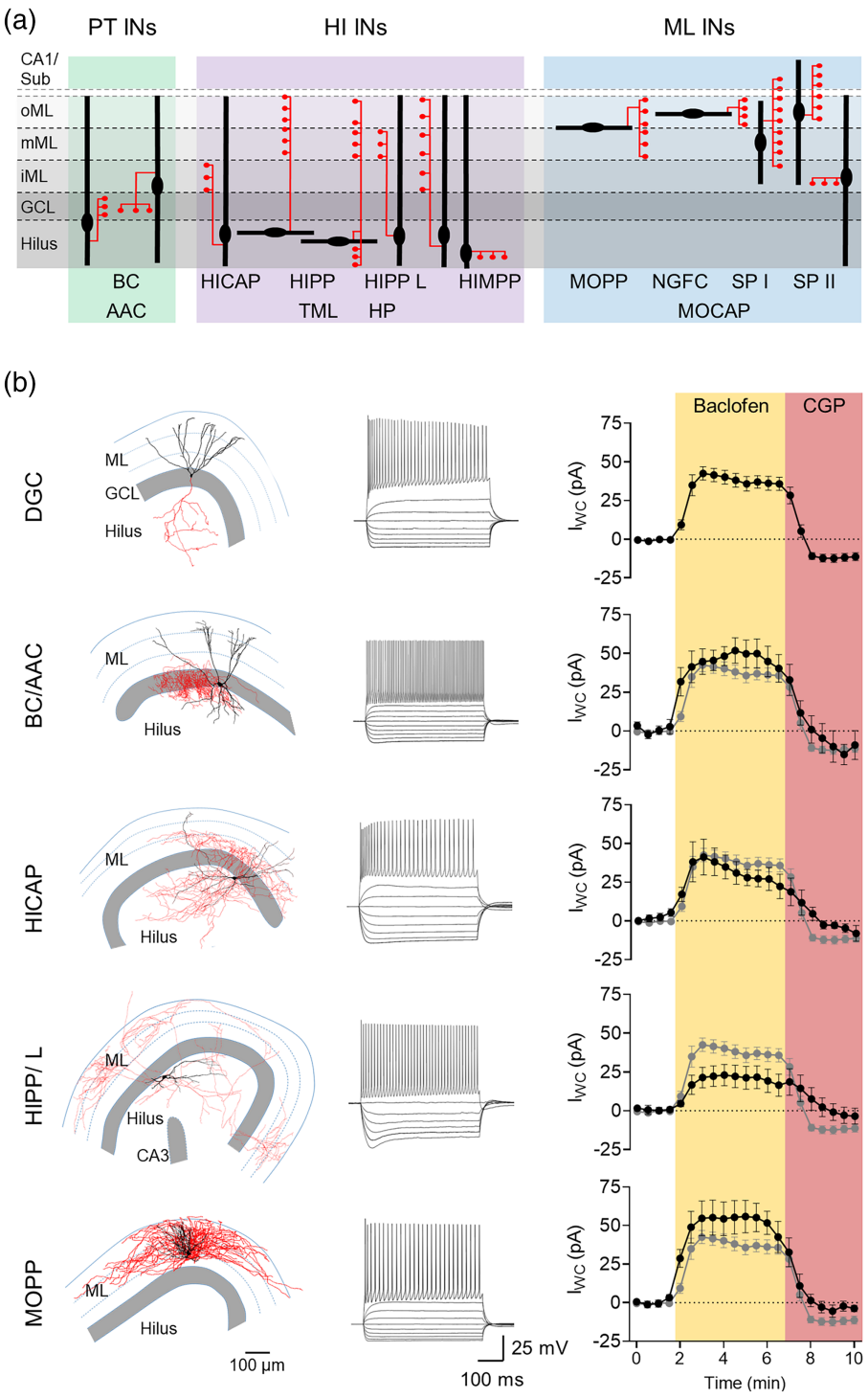

FIGURE 1 Postsynaptic $GABA_B$-receptor-mediated currents in dentate gyrus neurons. (a) Schematic overview of identified interneuron (IN) types in the dentate gyrus (DG) with their axonal and dendritic distribution superimposed on the different layers of the DG. The somatodendritic domain is shown in black and the axon in red (modified from Degro et al., 2022). (b) Representative reconstructions of a DGC and selected DG IN types (*left*, representative reconstructions of the HICAP and HIPP/L type are modified from Degro et al., 2022) with their corresponding AP discharge pattern in response to a set of hyper-to depolarizing current pulses (−250 to 250 pA, 50 pA steps, followed by a single 500 pA pulse, 500 ms duration, *middle*) and the effect of baclofen and CGP application on I_{wc} (mean ± SEM) plotted against time (*right*). DGC: $n = 8$; BC/AAC: $n = 9$; HICAP: $n = 7$; HIPP/L: $n = 6$; MOPP: $n = 7$. The I_{wc} time- course of DGCs is superimposed in gray in each IN plot as reference. AAC, axo-axonic cell; AP, action potential; BC, basket cell; CA1, cornu ammonis 1; CA3, cornu ammonis 3; DGC, dentate granule cell; GCL, granule cell layer; HI, hilus; HICAP, hilar commissural–associational pathway associated cell; HIMPP, hilar medial perforant pathway associated cell; HIPP/ HIPP L, hilar perforant pathway associated (like) cell; HP, hilar projecting cell; iML, inner molecular layer; IN, interneuron; I_{wc}, whole-cell current; ML, molecular layer; mML, middle molecular layer; MOCAP, molecular layer commissural–associational pathway associated cell; MOPP, molecular layer perforant pathway associated cell; NGFC, neurogliaform cell; oML, outer molecular layer; PT, perisomatic targeting; SP I, subiculum projecting cell I; SP II, subiculum projecting cell II; Sub, subiculum; TML, total molecular layer cell.

cells, Wilcoxon signed-rank test, compared to peak current). A high degree of variability in desensitization was noted in DG INs ($H = 31.4$, $p = .0005$, KW; Figure 2d). In particular, BC/AACs showed a low level of baclofen current desensitization similar to DGCs (17.2% ± 19.8% reduction, $Z = 0.0$, $p > .99$, $n = 9$ cells, KW, Dunn's, compared to DGCs). Meanwhile, TML and HICAP cells displayed pronounced desensitization with a reduction from peak current of 61.6% ± 16.7% recorded in the TML type ($Z = 3.47$, $p = .005$, $n = 9$ cells, KW, Dunn's, compared to DGCs) and 33.1% ± 29.4% in the HICAP type ($Z = 1.10$, $p > .99$, $n = 7$ cells, KW, Dunn's, compared to DGCs). Given that TML and HICAP cells are known to express cholecystokinin (Degro et al., 2022; Houser, 2007), this is in good agreement with our previous observation of KCTD12-mediated desensitization in CA1 CCK INs (Booker et al., 2017). Modest (albeit statistically non-significant) desensitization of baclofen-induced currents was also observed in hilar projecting (HP, 41.8% ± 24.9% reduction, $W = 15.0$, $p = .06$, $n = 5$ cells, Wilcoxon signed-rank test, compared to max. current) and MOCAP cells (41.4% ± 1.7% reduction, $W = 6.0$, $p = .25$, $n = 3$ cells,

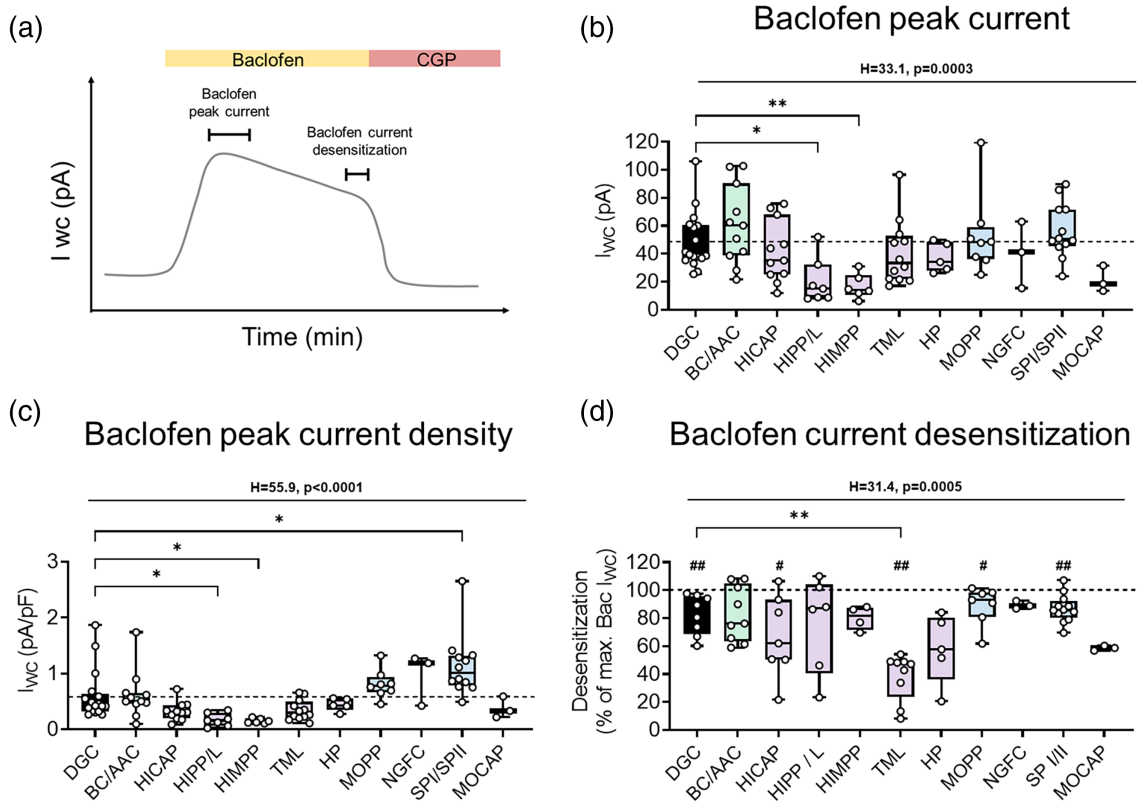

FIGURE 2 Baclofen-induced whole-cell peak currents and current desensitization. (a). Schematic of the change in I_{wc} in response to baclofen and CGP application plotted against time with indication of the peak current and current desensitization epoch. (b) Box-whisker plots (min. to max.) of the baclofen-induced peak current, baclofen-induced peak current-density (c) and baclofen current desensitization (d) of DGCs and DG IN types. Data from individual cells is shown overlaid. DGC: $n = 17$ (b), (c), $n = 8$ (d); BC/AAC: $n = 11$ (b), (c), $n = 9$ (d); HICAP: $n = 11$ (b), (c), $n = 7$ (d); HIPP/L: $n = 7$ (b), (c), $n = 6$ (d); HIMPP: $n = 6$ (b), (c), $n = 4$ (d); TML: $n = 12$ (b), (c), $n = 9$ (d); HP: $n = 5$; MOPP: $n = 8$ (b), (c), $n = 7$ (d); NGFC: $n = 3$; SP I/II: $n = 12$; MOCAP: $n = 3$. (b)–(d): *, $p < .05$; **, $p < .01$; Kruskal–Wallis test, Dunn's post-test. (d): #, $p < .05$; ##, $p < .01$; Wilcoxon signed rank test. AAC, axo-axonic cell; BC, basket cell; DG, dentate gyrus; DGC, dentate granule cell; HICAP, hilar commissural–associational pathway associated cell; HIMPP, hilar medial perforant pathway associated cell; HIPP/ HIPP L, hilar perforant pathway associated (like) cell; HP, hilar projecting cell; IN, interneuron; I_{wc}, whole-cell current; MOCAP, molecular layer commissural–associational pathway associated cell; MOPP, molecular layer perforant pathway associated cell; NGFC, neurogliaform cell; SP I, subiculum projecting cell I; SP II, subiculum projecting cell II; TML, total molecular layer cell.

Wilcoxon signed-rank test, compared to peak current). MOPP and SPI/II cells revealed a current desensitization of 10.9% ± 13.8% ($W = 26.0$, $p = .03$, $n = 7$ cells, Wilcoxon signed-rank test, compared to max. current) and 13.1% ± 10.0% ($W = 72.0$, $p = .002$, $n = 12$ cells, Wilcoxon signed-rank test, compared to max. current), respectively. Taken together, these data suggest that different DG INs express functional postsynaptic $GABA_B$Rs, but show cell type-specific variability in the magnitude of the induced currents as well as in desensitization.

3.2 | Photorelease of caged GABA activates postsynaptic $GABA_B$Rs and confirms cell type-specific differences in DG INs

To determine whether $GABA_B$R-mediated currents can be elicited by the endogenous ligand GABA, we next performed recordings in a subset of IN types employing focal photorelease of caged-GABA (Degro et al., 2015). For these experiments, 20 μM Rubi-GABA was bath-applied for 5 minutes and epifluorescent illumination by 470 nm light was applied for 200 ms at 2 minute intervals, centered over the cell soma (Figure 3a). Photorelease of GABA over the perisomatic domain produced slow uncaging inhibitory postsynaptic currents (uIPSC) in DGCs and all IN types, albeit with differing amplitudes ($H = 11.5$, $p = .02$, KW; Figure 3b, c). The average uIPSC of DGCs was (34.1 ± 21.5 pA, $n = 6$ cells). Consistent with whole-cell pharmacological activation, uIPSCs produced in BC/AACs had a similar, albeit higher amplitude (60.6 ± 25.5 pA, $Z = 1.37$, $p = .68$, $n = 4$ cells, KW, Dunn's, compared to DGCs). Similarly large uIPSCs were observed in MOPP type cells (67.8 ± 58.9 pA, $Z = 1.10$, $p > .99$, $n = 5$ cells, KW, Dunn's, compared to DGCs), whereas smaller uIPSCs than DGCs were measured in the HIPP/L type (6.7 ± 3.2 pA, $Z = 1.94$, $p = .21$, $n = 4$ cells, KW, Dunn's, compared to DGCs). In HICAP cells ($n = 4$ cells), the mean uIPSC amplitude was 30.5 ± 17.4 pA, similar to DCGs ($Z = 0.06$, $p > .99$, KW, Dunn's). When normalized to capacitance, the uIPSC current-density recapitulated IN-type differences ($H = 14.3$, $p = .007$,

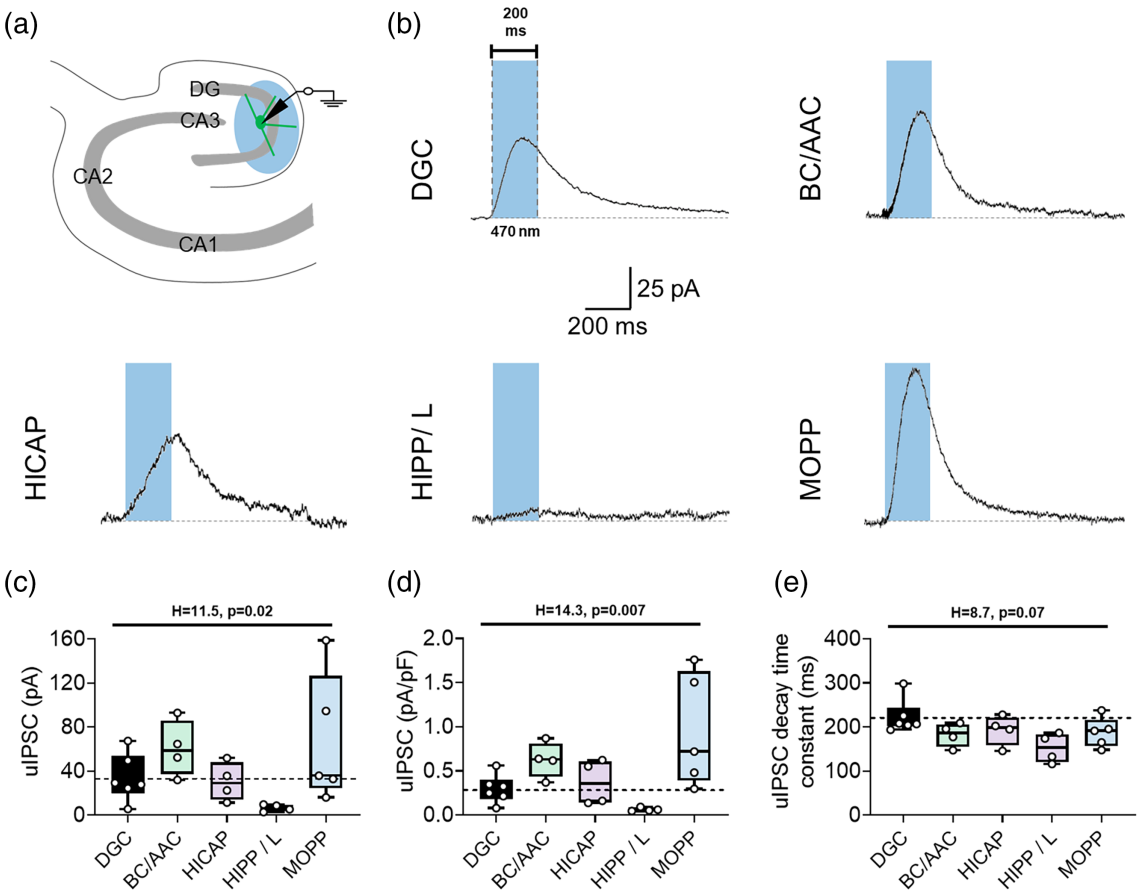

FIGURE 3 Activation of postsynaptic $GABA_B$-receptors via photorelease of caged-GABA. (a). Schematic overview of the experimental setup with neuron, recording pipette, and illumination field. (b). Representative traces of $GABA_B$-receptor-mediated inhibitory postsynaptic currents following uncaging of GABA (uIPSCs) of DGCs and selected DG IN types. Blue bar denotes the illumination time (200 ms) and wavelength (470 nm). (c). Box-whisker plots (min. to max.) of the measured uIPSC, uIPSC density, (d) and uIPSC decay-time constant (e) of DGCs and selected DG IN types. Data from individual cells is shown overlaid. DGC: $n = 6$; BC/AAC: $n = 4$; HICAP: $n = 4$; HIPP/L: $n = 4$; MOPP: $n = 5$. (c)–(e): Kruskal–Wallis test, Dunn's post-test. AAC, axo-axonic cell; BC, basket cell; CA1-3, *cornu ammonis* 1–3; DG, dentate gyrus; DGC, dentate granule cell; HICAP, hilar commissural–associational pathway associated cell; HIPP/ HIPP L, hilar perforant pathway associated (like) cell; IN, interneuron; MOPP, molecular layer perforant pathway associated cell.

KW; Figure 3d). The current-density in DGCs was 0.30 ± 0.16 pA/pF, which was statistically similar to that measured in BC/AACs (0.62 ± 0.20 pA/pF, $Z = 1.71$, $p = .35$, KW, Dunn's), MOPP cells (0.95 ± 0.64 pA/pF, $Z = 1.90$, $p = .23$, KW, Dunn's) and HICAP cells (0.37 ± 0.25 pA/pF, $Z = 0.34$, $p > .99$, KW, Dunn's). As for absolute currents, the uIPSC current-density for HIPP/L cells was smaller than for DGCs, albeit not significantly so (0.06 ± 0.02 pA/pF, $Z = 1.66$, $p = .39$, KW, Dunn's). We observed minimal difference in the measured decay-time constant of uIPSCs between all cell groups ($H = 8.7$, $p = .07$, KW; Figure 3e).

3.3 | Synaptic release of GABA can activate postsynaptic $GABA_B$Rs in DG INs

To confirm whether synaptic release of endogenous GABA is sufficient to activate postsynaptic $GABA_B$Rs in DG INs, we next performed electrical stimulation experiments in a subset of cell types (Figure 4). For these recordings, we placed a monopolar stimulating electrode in the outer ML in the presence of DNQX, DL-AP5, and Gabazine. In DGCs, delivery of 1×, 3×, or 5× stimuli (50 V amplitude, 200 Hz trains) resulted in incrementally larger IPSCs (Figure 4a), with a mean peak amplitude of 76.1 ± 23.4 pA (5 stimuli, $n = 10$ cells) and a mean decay-time constant of 236.1 ± 25.4 ms. The slow IPSCs were abolished by CGP application. By comparison, stimulus-evoked $GABA_B$R-mediated IPSCs were markedly smaller in all tested INs ($H = 13.1$, $p = .005$, KW; Figure 4e). BC/AACs possessed smaller IPSCs than that of DGCs, with a peak amplitude of 16.3 ± 6.8 pA ($Z = 3.02$, $p = .008$, $n = 11$ cells, KW, Dunn's, compared to DGCs; Figure 4b, e). Likewise, HICAP cells also had smaller IPSCs than DGCs, with a mean amplitude of 13.6 ± 5.8 pA ($Z = 3.20$, $p = .004$, $n = 9$ cells, KW, Dunn's, compared to DGCs; Figure 4c, e). For TML cells, IPSCs had a smaller (but not statistically different) IPSC amplitude of 22.4 ± 9.8 pA ($Z = 1.97$, $p = .15$, $n = 6$ cells, KW, Dunn's, compared

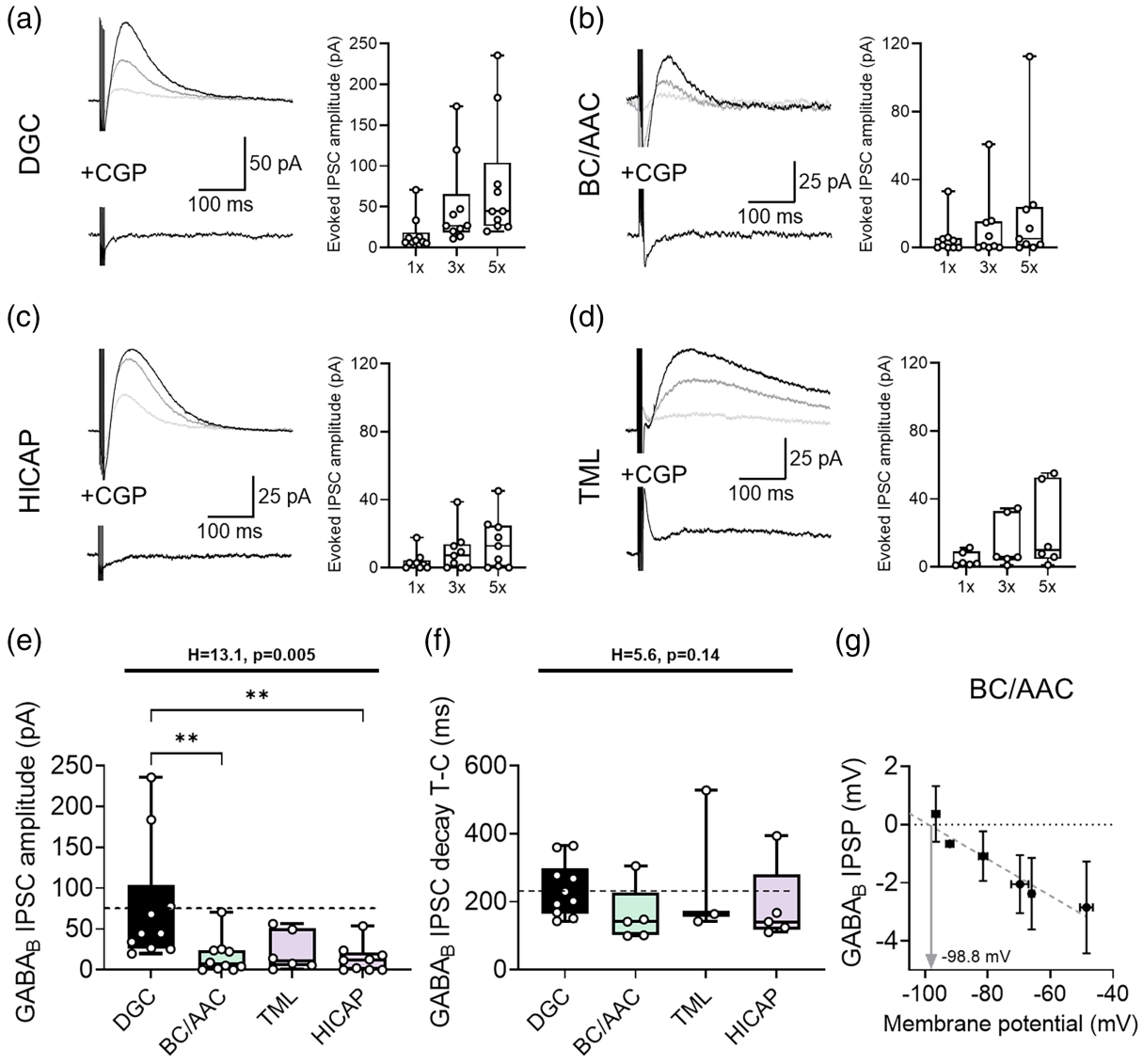

FIGURE 4 Release of endogenous GABA via electrical stimulation activates postsynaptic $GABA_B$-receptors on DGCs and DG INs. (a) Example recording from a DGC in the presence of DNQX, AP-5, and Gabazine from $V_m = -65$ mV. Following stimulation of oML with either 1, 3, or 5 stimuli, at 50 V (200 Hz) slow IPSCs were observed, which were blocked by bath application of CGP-55,845 (lower). Quantification of IPSC amplitude (box-whisker plots, min. to max.) following different stimuli numbers in all recorded DGCs ($n = 10$). Data from individual cells is shown overlaid (open circles). (b) The same data, but for identified BC/AACs ($n = 9$). (c). The same data, but for HICAP cells ($n = 9$). (d) The same data, but for TML cells ($n = 6$). (e) Comparison of the amplitude of $GABA_B$-receptor-mediated IPSCs in response to 5 stimuli in all cell types tested (box-whisker plots, min. to max.). Note, 2 BC/AACs were included additionally, but they did not receive 1 or 3 stimuli. (f) Comparison of $GABA_B$-receptor-mediated IPSC decay-time constant (T-C) for all IPSCs >5 pA (box-whisker plots, min. to max.). (g) Measured $GABA_B$-receptor-mediated IPSP amplitudes from BC/AACs ($n = 3$), where the membrane potential was held at hyper- to depolarized levels (mean ± SD). Note the estimated E_R[$GABA_B$-receptor] of −98.8 mV. Data from individual cells is shown overlaid. DGC: $n = 10$ (e), (f); BC/AAC: $n = 11$ (e), $n = 5$ (f); TML: $n = 6$ (e), $n = 3$ (f); HICAP: $n = 9$ (e), $n = 5$ (f). (e), (f): **, $p < .01$; Kruskal–Wallis test, Dunn's post-test. AAC, axo-axonic cell; BC, basket cell; DG, dentate gyrus; DGC, dentate granule cell; E_R, reversal potential; HICAP, hilar commissural–associational pathway associated cell; IN, interneuron; IPSC, inhibitory postsynaptic current; IPSP, inhibitory postsynaptic potential; oML, outer molecular layer; TML, total molecular layer cell.

to DGCs; Figure 4d, e). We observed no overt difference in evoked IPSC decay-time constants ($H = 5.6$, $p = .14$, KW; Figure 4f). To confirm that $GABA_B$R-mediated currents were underlain by Kir3 channels, we elicited IPSCs in a subset of BC/AACs ($n = 3$ cells), which revealed a reversal potential of −98.8 mV; consistent with this current being K^+-mediated (Figure 4g).

These data confirm that $GABA_B$Rs are recruited in DG INs by endogenous GABA release in the ML. The evoked release of

endogenous GABA largely confirms IN-type differences in postsynaptic $GABA_BR$ signaling.

3.4 | Activation of $GABA_BRs$ controls AP firing and directly affects membrane properties of DG IN types

Activation of postsynaptic $GABA_BRs$ typically leads to Kir3 channel opening, which dramatically shifts the passive membrane properties of neurons to reduce excitability (Dutar & Nicoll, 1988). Therefore, we next investigated whether differential $GABA_BR$ current density alters the excitability and AP discharge of DG INs in a cell type-specific manner. To address this, we applied trains of hyper- to depolarizing current steps (−250 pA to 250 pA, 50 pA steps, 500 ms duration) followed by a single depolarizing stimulus of 500 pA in current-clamp recordings (Figure 5a). The electrophysiological properties of different DG INs were measured during control conditions and following 10 μM baclofen and subsequent 5 μM CGP bath application.

In BCs/AACs ($n = 4$ cells), following baclofen application, we observed a tendency toward reduced AP discharge (Figure 5b), which was associated with a pronounced hyperpolarization of 5.4 ± 1.2 mV ($Q = 8.0$, $p = .005$, Friedman test, Figure 5c), a 12% reduction in measured R_{in} ($Q = 7.6$, $p = .02$, Friedman test, Figure 5d), and a tendency to reduce the slope of the frequency/current slope (FI, $Q = 5.2$, $p = .07$, Friedman test, Figure 5e) compared to control conditions. These baclofen-mediated effects were reversed by subsequent CGP application. Contrastingly, in HICAP cells ($n = 4$ cells), which possessed lower $GABA_BR$-mediated current- densities, we observed almost no modulation of AP discharge, no change in V_m ($Q = 3.5$, $p = 0.27$, Friedman test), in R_{in} ($Q = 4.8$, $p = .12$, Friedman test), nor FI slope ($Q = 3.5$, $p = .27$, Friedman test). Subsequent CGP application did not have any effect on HICAP excitability either. HIPP/L cells had the lowest $GABA_BR$ current-density, and accordingly also displayed minimal modulation of AP discharge ($n = 5$ cells), V_m ($Q = 4.8$, $p = .12$, Friedman test), R_{in} ($Q = 2.3$, $p = .43$, Friedman test) and FI slope ($Q = 2.8$, $p = .37$, Friedman test) with no observed effect of CGP. MOPP cells, which displayed a $GABA_BR$ current-density similar to that of DGCs, also showed a reduction in excitability following baclofen application ($n = 5$ cells). This was associated with an 8.0 ± 3.2 mV hyperpolarization of the neuronal membrane ($Q = 8.4$, $p = .009$, Friedman test), a 15.2% reduction in R_{in} ($Q = 8.0$, $p = .02$, Friedman test), and a prominent reduction in FI slope ($Q = 7.1$, $p = .02$, Friedman test). The excitability of MOPP cells was fully recovered following bath application of CGP. The properties of other DG IN types following baclofen and CGP application are shown in Supporting Information Figure 3.

These data demonstrate that there is a strong correlation of $GABA_BR$ current-density with neuronal excitability following receptor

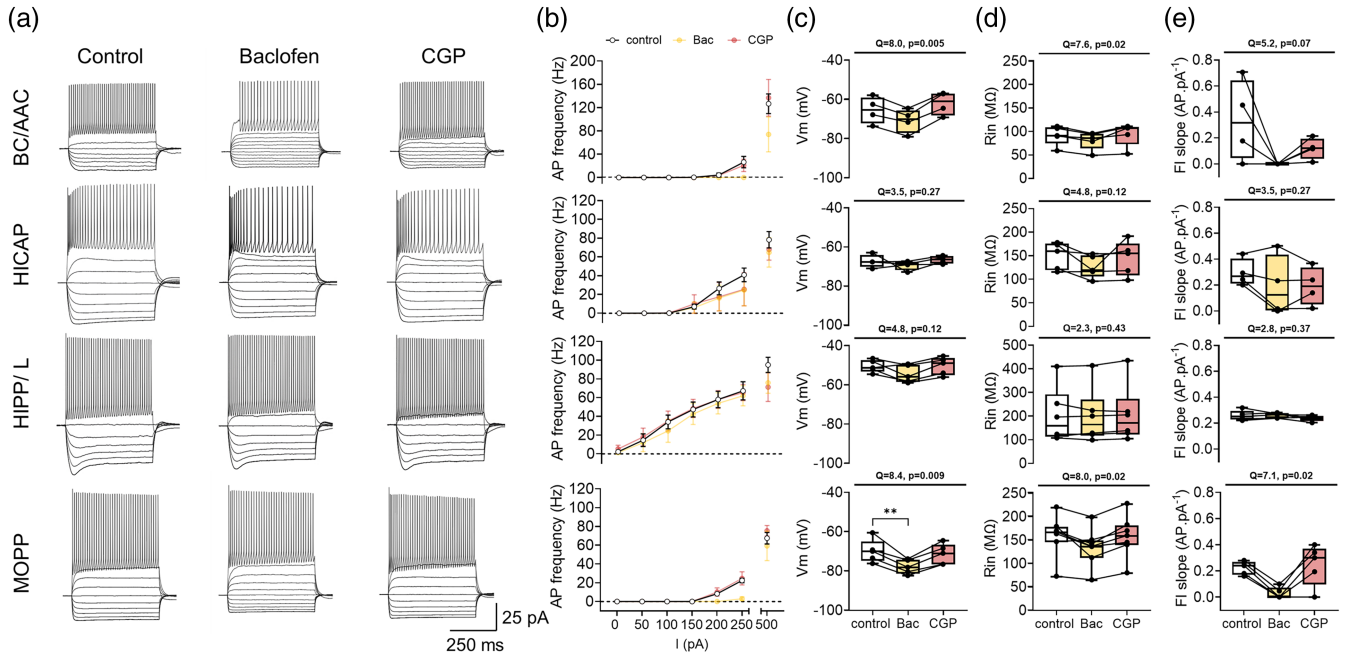

FIGURE 5 Changes of AP firing discharge, intrinsic membrane properties and frequency/current slope of DG IN types in response to postsynaptic $GABA_B$-receptor activation. (a) Representative traces of AP firing discharge in response to a set of hyper-to depolarizing current pulses (−250 to 250 pA, 50 pA steps, followed by a single 500 pA pulse, 500 ms duration) under control conditions and after baclofen and CGP application in the BC/AAC type, HICAP type, HIPP/L type and MOPP type with their corresponding current-firing response plot (−250 pA to 500 pA, mean ± SEM; b). IN type-specific box-whisker plots (min. to max.) of the changes in V_m (c), R_{in} (d), and of the change in frequency/current slope (FI, e) after baclofen and CGP application. BC/AAC: $n = 4$ (b), (c), (e), $n = 5$ (d); HICAP: $n = 4$ (b), (c), (e), $n = 5$ (d); HIPP/L: $n = 5$ (b), (c), (e), $n = 6$ (d); MOPP: $n = 5$ (b), (c), (e), $n = 7$ (d). (c)–(e): **, $p < .01$; Friedman test, Dunn's post-test. AAC, axo-axonic cell; AP, action potential; BC, basket cell; DG, dentate gyrus; HICAP, hilar commissural–associational pathway associated cell; HIPP/ HIPP L, hilar perforant pathway associated (like) cell; IN, interneuron; MOPP, molecular layer perforant pathway associated cell. R_{in}, input resistance; V_m, resting membrane potential.

activation. This confirms that BC/AAC and MOPP cells are likely strongly inhibited by $GABA_BRs$ when ambient levels of GABA are elevated, such as during periods of heightened network activity. HICAP cells displayed minimal baclofen modulation of excitability, despite mid-range $GABA_BR$ current-density, which may reflect the higher receptor desensitization profiles of this cell type.

4 | DISCUSSION

In this study, we show that functional $GABA_BRs$, like coupled to Kir3 channels are differentially expressed in the diverse array of DG INs. These receptors are localized to the somatodendritic region and are activated by the release of endogenous GABA. Ultimately, $GABA_BR$-mediated currents are sufficient to control the spike output of DG INs in a cell type-specific manner in response to sustained depolarization.

4.1 | Postsynaptic $GABA_BR$-mediated currents are present in DG INs across all layers

$GABA_BR$-mediated currents have been described throughout the nervous system and are known to be critically involved, beyond the control of neuronal excitability, in the induction and maintenance of synaptic plasticity, regulation of network oscillations (Brown et al., 2007), and ultimately behavioral performance (Brucato et al., 1996); in both rodents and humans (McDonnell et al., 2007). Functional postsynaptic $GABA_BRs$ have been well-studied in DGCs (Degro et al., 2015; Gonzalez et al., 2018; Lüscher et al., 1997; Mott et al., 1999). While diverse $GABA_BR$-mediated currents have been identified in some DG INs previously (Mott et al., 1999), our current study systematically compares functional currents across a greater diversity of IN types. We have previously shown that different classes of INs in the CA1 region of the hippocampus possess divergent magnitudes of $GABA_BR$ conductance, with PT cells (e.g., BC/AAC) typically having a current-density similar to that of neighboring PCs, and larger than dendritic-targeting INs (reviewed in Kulik et al., 2018). Our current data suggests that such a dichotomy is largely conserved in the rat DG. Exceptions to this general pattern were observed in the MOPP, NGFC, and SP I/II types. Indeed, evidence for large amplitude $GABA_BR$-mediated currents has been shown for NGFCs in CA1 and other cortical regions (Armstrong et al., 2011; Oláh et al., 2007; Price et al., 2008). The net effect of these $GABA_BR$-mediated currents will be to hyperpolarize DG INs, either through Kir3 channel activation (Degro et al., 2015) or potentially through other K^+ channels (Breton & Stuart, 2017).

Our data suggests that (with few exceptions) $GABA_BR$-mediated currents in DG INs show modest desensitization (Ulrich & Bettler, 2007). One exception to this was in DG INs that typically express CCK (e.g., TML, HICAP), where baclofen-induced currents tended to desensitize at a greater rate than for other INs and DGCs. This is in good agreement with a high expression of KCTD auxiliary subunits in CCK INs (Booker et al., 2017; Fritzius et al., 2017; Zheng et al., 2019). Consistent with activation of postsynaptic Kir3 channels, we observed reversal potentials of ~−100 mV (Sodickson & Bean, 1996) and dampening of neuronal excitability (Dutar & Nicoll, 1988) following $GABA_BR$ activation. We provide direct evidence that IN-type specific differences in $GABA_BR$ current-density relate to differing baclofen-induced changes in neuronal activity. Such neuronal responses to baclofen are likely dependent on the dendritic properties of IN subtypes, which often display unique passive properties (Nörenberg et al., 2010). Further work is needed to understand how dynamic regulation of $GABA_BRs$ *in vivo* contribute to the excitability (and thus timing) of IN recruitment. Finally, the kinetics of $GABA_BR$-mediated IPSC decay-time constants were largely similar between DG INs and DGCs. However, when the decay-time constants of all DG INs were pooled together, they were significantly faster than DGCs, in line with previous reports (Mott et al., 1999).

We have previously shown that very small or no postsynaptic $GABA_BR$-mediated outward currents are observed in somatostatin-expressing INs, where these postsynaptic receptors preferentially inhibit L-type calcium channels (rather than activating Kir3 channels) to control the induction of long-term potentiation (Booker et al., 2018). Interestingly, in contrast to CA1, we consistently observed $GABA_BR$-mediated currents in somatostatin-expressing HIPP/L cells, albeit substantially smaller than in DGCs and other INs. This may provide further evidence for potential hippocampal subfield-specific differences in somatostatin IN function (Hainmueller et al., 2024). Given the role of these HIPP/L cells in pattern separation in the rodent DG (Morales et al., 2021) this may indicate that $GABA_BRs$ could control their long-term recruitment and ability to tune spatial information. Evidence for such a role is indicated by the ability of baclofen to modulate grid cell activity in the DG (Foster et al., 2013) and its ability to impair spatial navigation (Brucato et al., 1996; McNamara & Skelton, 1996). Further studies will be crucial to fully understand the role of $GABA_BRs$ in microcircuit-level computations leading to spatial information transfer.

The source of GABA that recruits $GABA_BRs$ in DG INs remains elusive. Indeed, in our data, while many DG INs possessed high baclofen-induced current-densities and large amplitude uIPSCs in the perisomatic domain, stimulation of GABA release in the outer ML produced only small amplitude IPSCs in most DG INs (as compared to DGCs). This likely reflects the lower proportion of dendrites found in the ML of the IN types tested, with DGCs having >95% of dendrites in ML, while BC/AAC, TML, and HICAP cells possessing 60% or less of dendritic arbors in this layer (Degro et al., 2022). Baclofen application overcomes these differences, due to it being applied to the bath, thus likely activating all dendritic domains equally and allowing for quantification of total $GABA_BR$ current-density.

A further explanation for this is that the source of GABA originates from a variety of sources, via volume transmission (Booker et al., 2013; Davies et al., 1991; Gonzalez et al., 2018; Scanziani, 2000). It has previously been assumed that the main source of $GABA_BR$ signaling is NGFCs, which themselves are strongly modulated by $GABA_BRs$ (Armstrong et al., 2011; Oláh et al., 2007; Price et al., 2008). Our data, in particular from HI INs, indicates that this is

unlikely to be the only source of such GABA - as these DG INs have their somatodendritic domains far from the axonal arbors of NGFCs (Degro et al., 2022; Yuan et al., 2017). Meanwhile, the location of high densities of NGFCs overlaps with the dendrites of many IN types and DGCs which express higher $GABA_BR$ current densities. Determining how different INs contribute to the volume transmission of GABA in DG microcircuits is key knowledge to unlock how $GABA_BRs$ may be recruited during ongoing local circuit activity.

In summary, we provide compelling evidence for diversity of $GABA_BR$ signaling in DG INs, which largely confirms the cell type-specific nature of these currents in other brain regions. These data have direct implications for how we consider the timing and strength of different IN populations during circuit activity, and how slow inhibition may regulate spatial information transfer.

ACKNOWLEDGMENTS

We would like to thank Ina Wolter, Hieke Heilman, and Felix Bolduan with their technical and analytical support for this study. Also the members of AG Vida past and present for their support and discussions. In particular, we wish to thank our funders (IV: DFG VI 353/1-2, VI 353/4-1; SAB: Simons Initiative for the Developing Brain [SFARI: 529085]).

CONFLICT OF INTEREST STATEMENT

We confirm that none of the authors have any known conflicts of interest.

DATA AVAILABILITY STATEMENT

All data will be made available upon reasonable request.

ORCID

Imre Vida https://orcid.org/0000-0003-3214-2233
Sam A. Booker https://orcid.org/0000-0003-1980-9873

REFERENCES

Armstrong, C., Szabadics, J., Tamás, G., & Soltesz, I. (2011). Neurogliaform cells in the molecular layer of the dentate gyrus as feed-forward γ-aminobutyric acidergic modulators of entorhinal-hippocampal interplay. *Journal of Comparative Neurology*, *519*(8), 1476–1491.

Bartos, M., Vida, I., Frotscher, M., Geiger, J. R., & Jonas, P. (2001). Rapid signaling at inhibitory synapses in a dentate gyrus interneuron network. *Journal of Neuroscience*, *21*(8), 2687–2698.

Bartos, M., Vida, I., & Jonas, P. (2007). Synaptic mechanisms of synchronized gamma oscillations in inhibitory interneuron networks. *Nature Reviews Neuroscience*, *8*(1), 45–56.

Bettler, B., Kaupmann, K., Mosbacher, J., & Gassmann, M. (2004). Molecular structure and physiological functions of GABAB receptors. *Physiological Reviews*, *84*(3), 835–867.

Booker, S. A., Althof, D., Gross, A., Loreth, D., Müller, J., Unger, A., Fakler, B., Varro, A., Watanabe, M., & Gassmann, M. (2017). KCTD12 auxiliary proteins modulate kinetics of GABAB receptor-mediated inhibition in cholecystokinin-containing interneurons. *Cerebral Cortex*, *27*(3), 2318–2334.

Booker, S. A., Gross, A., Althof, D., Shigemoto, R., Bettler, B., Frotscher, M., Hearing, M., Wickman, K., Watanabe, M., & Kulik, Á. (2013). Differential GABAB-receptor-mediated effects in perisomatic-and dendrite-targeting parvalbumin interneurons. *Journal of Neuroscience*, *33*(18), 7961–7974.

Booker, S. A., Harada, H., Elgueta, C., Bank, J, Bartos, M., Kulik, A., & Vida, I. (2020). Presynaptic GABAB receptors functionally uncouple somatostatin interneurons from the active hippocampal network. *eLife*, *9*, e51156.

Booker, S. A., Loreth, D., Gee, A. L., Watanabe, M., Kind, P. C., Wyllie, D. J., Kulik, A., & Vida, I. (2018). Postsynaptic GABABRs inhibit L-type calcium channels and abolish long-term potentiation in hippocampal somatostatin interneurons. *Cell Reports*, *22*(1), 36–43.

Booker, S. A., Song, J., & Vida, I. (2014). Whole-cell patch-clamp recordings from morphologically-and neurochemically-identified hippocampal interneurons. *Journal of Visualized Experiments*, *30*(91), e51706.

Booker, S. A., & Vida, I. (2018). Morphological diversity and connectivity of hippocampal interneurons. *Cell and Tissue Research*, *373*(3), 619–641.

Borzello, M., Ramirez, S., Treves, A., Lee, I., Scharfman, H., Stark, C., Knierim, J. J., & Rangel, L. M. (2023). Assessments of dentate gyrus function: Discoveries and debates. *Nature Reviews Neuroscience*, *24*, 1–16.

Breton, J. D., & Stuart, G. J. (2017). GABAB receptors in neocortical and hippocampal pyramidal neurons are coupled to different potassium channels. *European Journal of Neuroscience*, *46*(12), 2859–2866.

Brown, J. T., Davies, C. H., & Randall, A. D. (2007). Synaptic activation of GABAB receptors regulates neuronal network activity and entrainment. *European Journal of Neuroscience*, *25*(10), 2982–2990.

Brucato, F., Levin, E., Mott, D., Lewis, D., Wilson, W., & Swartzelder, H. (1996). Hippocampal long-term potentiation and spatial learning in the rat: Effects of GABAB receptor blockade. *Neuroscience*, *74*(2), 331–339.

Canning, K. J., & Leung, L. S. (2000). Excitability of rat dentate gyrus granule cells in vivo is controlled by tonic and evoked GABAB receptor-mediated inhibition. *Brain Research*, *863*(1–2), 271–275.

Davies, C. H., Starkey, S. J., Pozza, M. F., & Collingridge, G. L. (1991). GABAB autoreceptors regulate the induction of LTP. *Nature*, *349*(6310), 609–611.

Degro, C. E., Bolduan, F., Vida, I., & Booker, S. A. (2022). Interneuron diversity in the rat dentate gyrus: An unbiased in vitro classification. *Hippocampus*, *32*(4), 310–331.

Degro, C. E., Kulik, A., Booker, S. A., & Vida, I. (2015). Compartmental distribution of GABAB receptor-mediated currents along the somatodendritic axis of hippocampal principal cells. *Frontiers in Synaptic Neuroscience*, *7*, 6.

Dutar, P., & Nicoll, R. (1988). A physiological role for GABAB receptors in the central nervous system. *Nature*, *332*(6160), 156–158.

Fernández-Ruiz, A., Oliva, A., Soula, M., Rocha-Almeida, F., Nagy, G. A., Martin-Vazquez, G., & Buzsáki, G. (2021). Gamma rhythm communication between entorhinal cortex and dentate gyrus neuronal assemblies. *Science*, *372*(6537), eabf3119.

Foster, J. D., Kitchen, I., Bettler, B., & Chen, Y. (2013). GABAB receptor subtypes differentially modulate synaptic inhibition in the dentate gyrus to enhance granule cell output. *British Journal of Pharmacology*, *168*(8), 1808–1819.

Freund, T. F., & Buzsáki, G. (1996). Interneurons of the hippocampus. *Hippocampus*, *6*(4), 347–470.

Fritzius, T., Turecek, R., Seddik, R., Kobayashi, H., Tiao, J., Rem, P. D., Metz, M., Kralikova, M., Bouvier, M., & Gassmann, M. (2017). KCTD hetero-oligomers confer unique kinetic properties on hippocampal GABAB receptor-induced K+ currents. *Journal of Neuroscience*, *37*(5), 1162–1175.

Gonzalez, J. C., Epps, S. A., Markwardt, S. J., Wadiche, J. I., & Overstreet-Wadiche, L. (2018). Constitutive and synaptic activation of GIRK channels differentiates mature and newborn dentate granule cells. *Journal of Neuroscience*, *38*(29), 6513–6526.

Guzman, S. J., Schlögl, A., & Schmidt-Hieber, C. (2014). Stimfit: Quantifying electrophysiological data with Python. *Frontiers in Neuroinformatics*, *8*. https://doi.org/10.3389/fninf.2014.00016

Hainmueller, T., Cazala, A., Huang, L.-W., & Bartos, M. (2024). Subfield-specific interneuron circuits govern the hippocampal response to novelty in male mice. *Nature Communications*, *15*(1), 714.

Hájos, N., & Mody, I. (2009). Establishing a physiological environment for visualized in vitro brain slice recordings by increasing oxygen supply and modifying aCSF content. *Journal of Neuroscience Methods*, *183*(2), 107–113.

Hosp, J. A., Strüber, M., Yanagawa, Y., Obata, K., Vida, I., Jonas, P., & Bartos, M. (2014). Morpho-physiological criteria divide dentate gyrus interneurons into classes. *Hippocampus*, *24*(2), 189–203.

Houser, C. R. (2007). Interneurons of the dentate gyrus: An overview of cell types, terminal fields and neurochemical identity. *Progress in Brain Research*, 217–811. https://doi.org/10.1016/s0079-6123(07)63013-1

Kulik, Á., Booker, S. A., & Vida, I. (2018). Differential distribution and function of GABABRs in somato-dendritic and axonal compartments of principal cells and interneurons in cortical circuits. *Neuropharmacology*, *136*, 80–91.

Kulik, Á., Nakadate, K., Nyíri, G., Notomi, T., Malitschek, B., Bettler, B., & Shigemoto, R. (2002). Distinct localization of GABAB receptors relative to synaptic sites in the rat cerebellum and ventrobasal thalamus. *European Journal of Neuroscience*, *15*(2), 291–307.

Kulik, Á., Vida, I., Luján, R., Haas, C. A., López-Bendito, G., Shigemoto, R., & Frotscher, M. (2003). Subcellular localization of metabotropic GABAB receptor subunits GABAB1a/b and GABAB2 in the rat hippocampus. *Journal of Neuroscience*, *23*(35), 11026–11035.

Longair, M. H., Baker, D. A., & Armstrong, J. D. (2011). Simple Neurite Tracer: Open source software for reconstruction, visualization and analysis of neuronal processes. *Bioinformatics*, *27*(17), 2453–2454.

Lüscher, C., Jan, L. Y., Stoffel, M., Malenka, R. C., & Nicoll, R. A. (1997). G protein-coupled inwardly rectifying K+ channels (GIRKs) mediate postsynaptic but not presynaptic transmitter actions in hippocampal neurons. *Neuron*, *19*(3), 687–695.

McDonnell, M. N., Orekhov, Y., & Ziemann, U. (2007). Suppression of LTP-like plasticity in human motor cortex by the GABA B receptor agonist baclofen. *Experimental Brain Research*, *180*, 181–186.

McNamara, R. K., & Skelton, R. W. (1996). Baclofen, a selective GABAB receptor agonist, dose-dependently impairs spatial learning in rats. *Pharmacology Biochemistry and Behavior*, *53*(2), 303–308.

Morales, C., Morici, J. F., Espinosa, N., Sacson, A., Lara-Vasquez, A., García-Pérez, M., Bekinschtein, P., Weisstaub, N. V., & Fuentealba, P. (2021). Dentate gyrus somatostatin cells are required for contextual discrimination during episodic memory encoding. *Cerebral Cortex*, *31*(2), 1046–1059.

Mott, D. D., & Lewis, D. V. (1991). Facilitation of the induction of long-term potentiation by GABAB receptors. *Science*, *252*(5013), 1718–1720.

Mott, D. D., Li, Q., Okazaki, M. M., Turner, D. A., & Lewis, D. V. (1999). GABAB-receptor-mediated currents in interneurons of the dentate-hilus border. *Journal of Neurophysiology*, *82*(3), 1438–1450.

Nörenberg, A., Hu, H., Vida, I., Bartos, M., & Jonas, P. (2010). Distinct non-uniform cable properties optimize rapid and efficient activation of fast-spiking GABAergic interneurons. *Proceedings of the National Academy of Sciences*, *107*(2), 894–899.

Oláh, S., Komlosi, G., Szabadics, J., Varga, C., Toth, E., Barzo, P., & Tamas, G. (2007). Output of neurogliaform cells to various neuron types in the human and rat cerebral cortex. *Frontiers in Neural Circuits*, *1*, 84.

Price, C. J., Scott, R., Rusakov, D. A., & Capogna, M. (2008). GABAB receptor modulation of feedforward inhibition through hippocampal neurogliaform cells. *Journal of Neuroscience*, *28*(27), 6974–6982.

Scanziani, M. (2000). GABA spillover activates postsynaptic GABAB receptors to control rhythmic hippocampal activity. *Neuron*, *25*(3), 673–681.

Schmidt-Hieber, C., & Nolan, M. F. (2017). Synaptic integrative mechanisms for spatial cognition. *Nature Neuroscience*, *20*(11), 1483–1492.

Sodickson, D. L., & Bean, B. P. (1996). GABAB receptor-activated inwardly rectifying potassium current in dissociated hippocampal CA3 neurons. *Journal of Neuroscience*, *16*(20), 6374–6385.

Spruston, N., & Johnston, D. (1992). Perforated patch-clamp analysis of the passive membrane properties of three classes of hippocampal neurons. *Journal of Neurophysiology*, *67*(3), 508–529.

Srivastava, V., Parker, D. J., & Edwards, S. F. (2008). The nervous system might 'orthogonalize' to discriminate. *Journal of Theoretical Biology*, *253*(3), 514–517. https://doi.org/10.1016/j.jtbi.2008.03.031

Uematsu, M., Hirai, Y., Karube, F., Ebihara, S., Kato, M., Abe, K., Obata, K., Yoshida, S., Hirabayashi, M., & Yanagawa, Y. (2008). Quantitative chemical composition of cortical GABAergic neurons revealed in transgenic venus-expressing rats. *Cerebral Cortex*, *18*(2), 315–330.

Ulrich, D., & Bettler, B. (2007). GABAB receptors: Synaptic functions and mechanisms of diversity. *Current Opinion in Neurobiology*, *17*(3), 298–303.

Vida, I., Bartos, M., & Jonas, P. (2006). Shunting inhibition improves robustness of gamma oscillations in hippocampal interneuron networks by homogenizing firing rates. *Neuron*, *49*(1), 107–117.

Yuan, M., Meyer, T., Benkowitz, C., Savanthrapadian, S., Ansel-Bollepalli, L., Foggetti, A., Wulff, P., Alcami, P., Elgueta, C., & Bartos, M. (2017). Somatostatin-positive interneurons in the dentate gyrus of mice provide local-and long-range septal synaptic inhibition. *eLife*, *6*, e21105.

Zheng, S., Abreu, N., Levitz, J., & Kruse, A. C. (2019). Structural basis for KCTD-mediated rapid desensitization of GABAB signalling. *Nature*, *567*(7746), 127–131.

SUPPORTING INFORMATION

Additional supporting information can be found online in the Supporting Information section at the end of this article.

How to cite this article: Degro, C. E., Vida, I., & Booker, S. A. (2024). Postsynaptic $GABA_B$-receptor mediated currents in diverse dentate gyrus interneuron types. *Hippocampus*, 1–12. https://doi.org/10.1002/hipo.23628